# Exploring mission design for imaging spectroscopy retrievals for land and aquatic ecosystems

**A. M. Raiho[1] [2], K. Cawse-Nicholson[3] , A. Chlus[3] , J. Dozier[4] , M. Gierach[3], K. Miner[3], F. Schneider[3], D. Schimel[3], S. Serbin[6], A. N. Shiklomanov[1], D. R. Thompson[3], P. A. Townsend[3] [5], S. Zareh[3], M. Skiles[7], B. Poulter[1]**

[1]NASA Goddard Space Flight Center, Biospheric Sciences Lab, Greenbelt, MD 20771
[2]Earth System Science Interdisciplinary Center, University of Maryland, College Park, MD 20740
[3]Jet Propulsion Laboratory, California Institute of Technology, Pasadena, CA 91109
[4]Bren School of Environmental Science & Management, University of California, Santa Barbara, CA 93106
[5]University of Wisconsin – Madison, , Department of Forest and Wildlife Ecology, 1630 Linden Drive, Madison, WI 53706 USA
[6]Brookhaven National Laboratory, Upton, NY 11973
[7]Department of Geography, University of Utah, Salt Lake City, UT 84112

Corresponding author: Ann Raiho (ann.m.raiho@nasa.gov)

**Key Points:**

- High spectral resolution (~10nm), high spatial resolution (~30m), and high revisit (less than 16 days) is needed to estimate Earth's geophysical properties with imaging spectroscopy and corresponding retrieval algorithms.
- We simulate the effects of instrument signal-to-noise ratios (SNR) on retrieval accuracy using a codebase called Hypertrace.
- Our approach provides a framework for current and future mission design planning.

## Abstract

The retrival algorithms used for optical remote sensing satellite data to estimate Earth's geophysical properties have specific requirements for spatial resolution, temporal revisit, spectral range and resolution, and instrument signal to noise ratio (SNR) performance to meet science objectives. Studies to estimate surface properties from hyperspectral data use a range of algorithms sensitive to various sources of spectroscopic uncertainty, which are in turn influenced by mission architecture choices. Retrieval algorithms vary across scientific fields and may be more or less sensitive to mission architecture choices that affect spectral, spatial, or temporal resolutions and spectrometer SNR. We used representative remote sensing algorithms across terrestrial and aquatic study domains to inform aspects of mission design that are most important for impacting accuracy in each scientific area. We simulated the propagation of uncertainties in the retrieval process including the effects of different instrument configuration choices. We found that retrieval accuracy and information content degrade consistently at >10 nm spectral resolution, >30 m spatial resolution, and >8 day revisit. In these studies, the noise reduction associated with lower spatial resolution improved accuracy vis à vis high spatial resolution measurements. The interplay between spatial resolution, temporal revisit and SNR can be quantitatively assessed for imaging spectroscopy missions and used to identify key components of algorithm performance and mission observing criteria.



## Plain Language Summary

Detailed observations of Earth's visible to shortwave infrared spectra, known as hyperspectral imagery or imaging spectroscopy, will provide novel insights across scientific disciplines. Vegetation, aquatic, mineral, and snow scientists have independently developed techniques for using hyperspectral imagery to measure different features of their targets. But, developing measurement objectives that will work well for every kind of measurement target is difficult. Here, we test several representative image analysis techniques to inform the planning process future hyperspectral missions. Specifically, we investigate the effect that changing the number of spectral bands, the size of image pixels, and the frequency of repeat observations has on each technique's accuracy.


## 1 Introduction

Global imaging spectroscopy from NASA's Surface Biology and Geology (SBG) designated observable will improve understanding of five focal areas of Earth Science: marine and terrestrial ecosystems, seasonal to centennial climate variability, weather and air quality, hydrology and water resources, and dynamics and hazards associated with Earth's surface and interior (National Academies of Sciences, Engineering, and Medicine, 2018; Schimel, Townsend and Pavlick, 2020). SBG will provide visible through shortwave-infrared reflectance (~380-2500 nm wavelengths) and thermal (4.5 to 12 μm) emissivity observations from space with global coverage, frequent revisit, and high spectral fidelity (Stavros et al., in press). Designing a successful mission that meets diverse scientific objectives requires evaluating alternative mission architectures (Thompson *et al*., 2021). In SGB's case, each science focal area depends on a different aspect of mission architecture for accuracy (Cawse-Nicholson *et al*., 2021). To characterize the scientific impact of trade-offs associated with different mission architectures, we illustrate the driving examples behind each focal area (Table 1) and assess the effects of measurement trades on a target retrieval.

Trade-offs are a fundamental component of mission design. Fundamental trade-offs associated with different mission architectures occur between spectral, spatial, and temporal resolutions and the radiometric precision of the instrument. Radiometric precision (i.e., signal-to-noise ratio or SNR) is a function of the number of photons an instrument receives. When integrating over a smaller spectral (i.e., higher spectral resolution) or spatial area (i.e., higher spatial resolution) at the fixed orbital speed of a spacecraft, fewer photons will reach the instrument, degrading SNR with downstream consequences for retrievals of geophysical variables. On the other hand, some features of interest require fine spectral and spatial resolution to be accurately retrieved. Mission architecture design must address how optimizing for high instrument SNR impacts spectral, spatial, and temporal resolution. For a mission like SBG, which covers a range of scientific disciplines, the trades between each of the three types of resolutions and SNR must be thoroughly evaluated using a consistent traceability framework.

Imaging spectroscopy (i.e., 100s to 1000s of contiguous wavelength channels) allows for more precise discrimination of Earth surface properties than multispectral imagery (i.e., 3 to 20 wavelength channels) because of the higher information content in these hyperspectral measurements (Thompson, Boardman, *et al.*, 2017; Cawse-Nicholson *et al.*, 2019). The spectral resolution of a hyperspectral image has been shown to greatly affect mineral (Swayze, 2003) and vegetation (Shiklomanov *et al.*, 2016) retrieval accuracy because these algorithms require fine spectrally resolved information. In both these cases, high spectral resolution may compensate for lower SNR by contributing more information content. Requirements also vary considerably by algorithm type . For example, snow retrieval algorithms are similar to common mineral retrieval algorithms that consider the spectral signature around known absorption wavelengths (Nolin and Dozier, 1993). As such, a stronger focus on fine spectral resolution is needed to discriminate and identify key mineral absorption features associated with specific mineral species or to identify or discriminate dust versus snow grain particles, as well as determine water content and age of snowpack (REFS). On the other, vegetation algorithms are typically based on statistical models (e.g., Partial Least Squares Regression, PLSR; Burnett et al., 2021) or physically-based models (e.g., radiative transfer model inversion) that relate plant properties at leaf or canopy level to more broad absorption features (e.g. Curran, 1989) and spectral information (Verrelst et al., 2019; Serbin and Townsend, 2020) As such, vegetation algorithms tend to require higher SNR or spatial resolution over very fine spectral resilution. Aquatic algorithms are especially sensitive to the additive atmospheric contribution to the spectral signal, and their retrieval accuracy may be particularly susceptible to degrading spectral resolution and the effects of low SNR because of how aquatic properties such as glint (Hu, 2011), bubbles (Dierssen, 2019), and optical variability in the water column (Garcia *et al.*, 2020) interact with water-leaving radiances. In our analyses, we demonstrate how retrieval algorithms that depend on hyperspectral imagery respond to the effects of degrading spectral resolution and radiometric precision on retrieval accuracy.

Holding SNR constant, finer spatial resolution or increased number of pixels per image will typically lead to higher information content in an image (Cawse-Nicholson *et al.*, 2019). However, instrument SNR decreases with finer spatial resolution because smaller pixels result in fewer photons received by each focal plane array detector element. A driving case for spatial resolution is the ecological focal area where different ecosystems have different dominanting spatial scale processes (Turner, Dale and Gardner, 1989; Wang *et al.*, 2018). For instance, a homogenous scenes (e.g., dense deciduous forest) may not require fine spatial detail to

understand plant functional traits while a heterogeneous scenes (e.g., sparse lower montane ecosystem) with a variety of ecosystem types may require fine spatial detail.

Frequent temporal revisit is another fundamental aspect of the mission architecture and provides a basis for quantifying the effects of natural disasters and seasonal phenomena (Schimel, Townsend and Pavlick, 2020). The ability to detect a short duration event (e.g., a volcanic eruption or mudslide) or frequent changes during a season (e.g., snow albedo) may be hindered by longer revisit time intervals or areas where cloud cover is common, or by overpass time. However, increasing revisit frequency can be obtained at the cost of spatial resolution and must be quantitatively justified.

To optimize for retrieval accuracy across five scientific areas, mission architecture design must consider tradeoffs between spectral, spatial, and temporal resolutions. In this study, we look at specific driving case studies to quantify the performance impacts of these design choices on the range of SBG science objectives. Specifically, we perform a simulation experiment in which we synthesize artificial imaging spectroscopy data and apply state of practice retrieval algorithms with varying sensor noise and resolution. Currently, high resolution hyperspectral time series data are uncommon, so our strategy is to show the probability of detecting an event depending on event duration and revisit time interval using simulated data. Our approach compares algorithm accuracy with and without instrument noise along gradients of coarsening resolutions to determine optimal resolutions for imaging spectroscopy architecture design.

## 2 Materials and Methods

Radiance measurements from hyperspectral missions will be converted into surface reflectance values through atmospheric correction, which isolates and removes the contribution of absorption and scattering from atmospheric aerosols, water vapor, and other components on the overall radiance signal, and provides estimates of incoming and outgoing radiation for each pixel at the Earth surface (Vermote and Kotchenova, 2008). In this study, we use an atmospheric correction approach that employs a physically based atmospheric radiative transfer model inversion. We use the Imaging Spectrometer Optimal FITting codebase (i.e., ISOFIT; Thompson *et al.*, 2018), whereby atmospheric and surface reflectance can be estimated jointly using optimal estimation (OE; Thompson *et al.*, 2018). Estimated surface reflectance from the OE procedure then provides the information for algorithms that retrieve geophysical properties. These algorithms can take many forms. The retrieval algorithms listed in Table 1 were chosen to span each of the five core scientific areas and were made available through collaborations with the algorithms working group.

### 2.1 Hypertrace and instrument modeling

We developed the Hypertrace simulation workflow to trace the hyperspectral data uncertainty pipeline from top of atmosphere radiance to bio- and geophysical retrievals (https://github.com/isofit/isofit/tree/master/examples/py-hypertrace). Operationally, Hypertrace starts from known surface reflectance and atmospheric conditions based on a specific spectral resolution, and then simulates top-of-atmosphere radiance and instrument radiances based on the proposed instrument design, and then performs atmospheric correction via optimal estimation to estimate surface reflectance.

Pragmatically, Hypertrace is a wrapper around the ISOFIT codebase (See: Brodrick et al, 2021) which provides both forward and inverse reflectance modeling for translation between reflectance and radiance. Our ISOFIT configuration files can be found in the supplemental materials. Hypertrace manages this simulation process at runtime, and applies geophysical retrieval algorithms to the estimated surface reflectance. Hypertrace is written in Python and can be configured with a simple JSON interface.

Hypertrace allows for the inclusion of different imaging spectrometer detector configurations that provide various SNR profiles (Figure 1). An imaging spectrometer includes the optical system and the detector. The optics include the telescope, a dispersive element such as a prism or diffraction grating, and the slit, the entrance width that determines photon throughput. In our experiments, we used configurations for two Chroma instruments (i.e., focal plane array) Instrument-A and Instrument-B detectors and also Hyperion, where Instrument-A has a detector pixel pitch of 0.0030 cm and a slit width of 30 microns while Instrument-B has a detector pixel pitch of 0.0018 cm and a slit width of 18 microns. We selected these Chroma spectrometers as examples because they have been used in the Earth Surface Mineral Dust Source Investigation (EMIT) mission, a similar imaging spectroscopy mission to SBG (Connelly *et al.*, 2021). We compare against Hyperion to show the abilities of our workflow to include SNR from both future and past instuments. These spectrometer settings as well as desired instrument spatial resolution alter the SNR along the visible to shortwave infrared (Figure 1).

For the Chroma instruments, we derived instrument SNR using the following approach. The SNR describes the ratio of the signal to noise for the given spatial resolution element, where the signal is defined as the total number of collected electrons per unit area (i.e. pixel) over the total noise for the same area. The signal is proportional to the following equation:

$$Signal = L * \delta\lambda * A_o * \Omega_d * t_{int} * T * \eta \quad (1)$$

Where L is spectral radiance at sensor, $\delta\lambda$ is the instrument's spectral resolution, $A_o$ is the instrument telescope aperture, $\Omega_d$ is the solid angle of the instrument, $t_{int}$ is the integration time per spatial sample, T is transmission, and $\eta$ is the detector quantum efficiency.

For a given spatial sample, the noise comes from multiple contributing factors, including the shot noise, read noise, dark noise, electronics noise and quantum noise.

$$\text{Noise} = \sqrt{N_{shot}^2 + N_{dark}^2 + N_{read}^2 + N_{electronics}^2} \quad (2)$$

The shot noise is usually the largest contributor to the noise and is a poissonian effect that is an inherent property of the photon collection pheonomenon in optical devices. The dark noise is the product of the dark current of the focal plane array and the integration times we work with. The read noise is associated with every frame read. For digital focal plane array like Instrument-B the electronics noise is zero while it is a non-zero value for

the analog version Instrument-A. Usually the focal plane array gets characterized in a laboratory thermal-vacuum chamber that allows the read noise, dark current, well capacity, linearity and crosstalk to be measured and chacraterized. The results of these characterizations are critical to the design and performance predictions of imaging spectrometers using the focal plane array.

For the Hyperion instrument, we used a parametric approach for calculating instrument SNR. First, we collected invariant scenes from early in the Hyperion campaign. We then used the radiance from the invariant scenes and the parameter noise estimation process from Bioucas-Dias and Nascimento, 2005 to derive SNR for Hyperion.

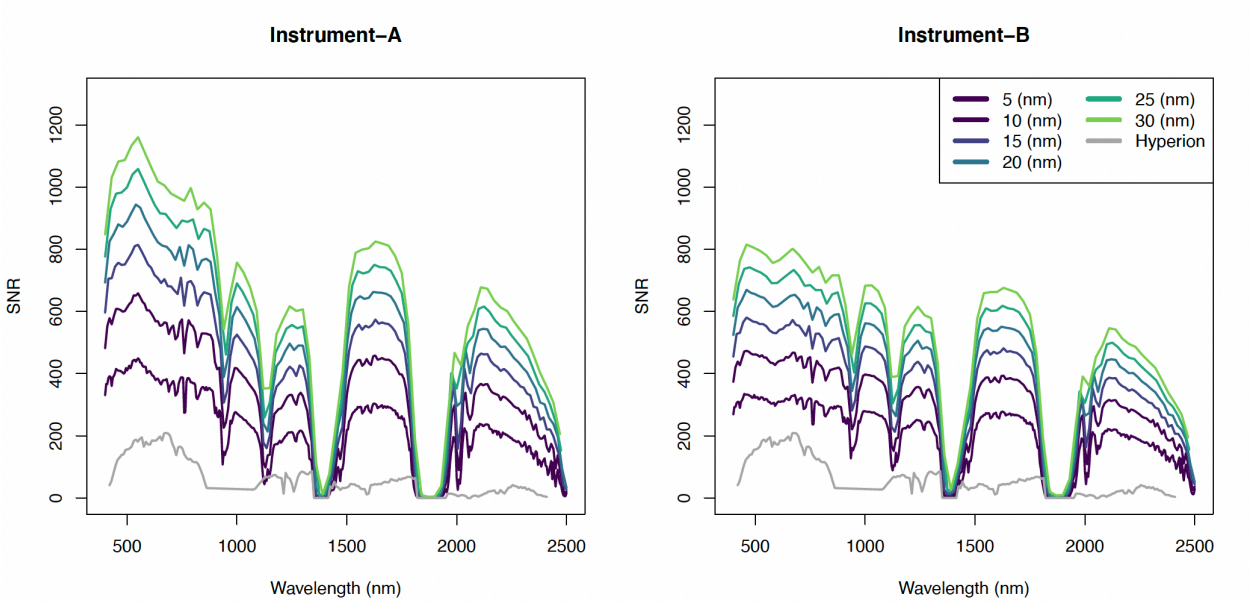


**Figure 1**: Instrument SNR over the visible and near-infrared (VNIR; 400 - 1000 nm) and short wave infrared (SWIR; 1000 - 2500 nm) for Instrument-A (left) and Instrument- (right) spectrometers colored by spatial resolution (m) range considered in this study. The vertical line in each panel represents the split between the VNIR and the SWIR.

## 2.2 Spectral and spatial sensitivity

Our simulation experiments have two parts: In 'direct' experiments, we apply retrieval algorithms to degraded reflectance data, and compare the outcome a similar retrieval at native resolution (Figure 2 black). In 'instrument' experiments, we degrade the radiance at sensor in Hypertrace using an instrument model, perform an atmospheric correction, and then apply the retrieval algorithm to the estimated surface reflectance. Therefore, only the instrument experiments include the effect of imperfect instrument radiometry ("noise"). We illustrate the concept behind our simulations in Figure 2. In the 'instrument' experiments, we consider two instrument models, representing state-of-the art detectors due to launch in the near future (EMIT, Connelly *et al.*, 2021). We use Hypertrace to simulate the contributions of imperfect radiometry in Instrument-A, Instrument-B, or Hyperion spectrometer to biases and uncertainties in the geophysical

variable of interest (Figure 2 red). We repeat the direct and instrument application steps along the resolution degradation range of interest. We then compare both the direct retrievals and the Hypertrace retrievals to the direct retrieval at the native resolution using a variety of standard validation statistics, e.g., root mean square error (RMSE) and kappa score (for categorical data) to illustrate the effects of degrading resolution on retrieval accuracy.

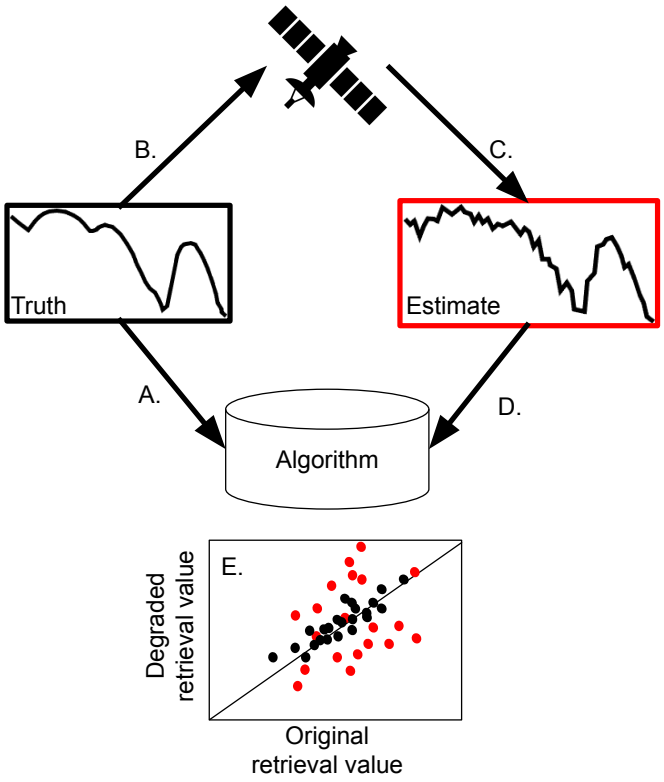


**Figure 2**: Conceptual diagram of one iteration of our analysis. A. True surface reflectance is used to obtain true or direct retrievals that are not affected by the noise (black). B. and C. True surface reflectance is run through hypertrace forward (B) and inverse (C) models to obtain estimated surface reflectance including uncertainties from atmospheric correction and instrument design signal to noise ratio (SNR). D. These estimated reflectances (red) are given to the same algorithms and then compared to the directly estimated retrievals (E).

We chose spectral and spatial resolution experiments to demonstrate accuracy degradation across the full range of current mission design choices and corresponding trades with SNR. In our spectral resolution experiments, we varied the bandwidth from 5nm to 30nm in 5nm increments, resulting in 6 experiments with a minimum of 70 bands and a maximum of 421 bands. Similarly, we varied spatial resolution from 20 m to 60 m by 10 m increments. We also included 100 m spatial resolution experiments to demonstrate algorithm accuracy at very low spatial resolutions. The scenes were resampled to coarser resolutions using Gaussian convolution aggregation for spectral resolution and bilinear averaging for spatial resolution (ignoring potential autocorrelation between spectral bands). We then repeated these experiments including the

238 corresponding effects of SNR shown in Figure 1 (See Figure 2 black versus red). All
239 experiments were conducted with 1000 randomly drawn points from each scene.

240 We chose representative hyperspectral scenes based on a set of science areas where
241 retrieval algorithms were available and provided by the algorithm developers (Table 1).
242 These scenes have been BRDF corrected and atmospherically corrected, meaning they
243 provide estimates of the hemispherical-directional reflectance factor (HDRF, *sensu*
244 Schaepman-Strub et al. 2006) for a nadir viewing angle. Table 1 lists the supporting
245 citations for each scene.

246 The algorithms use a variety of methods. Absorption feature matching uses specific
247 features of the reflectance spectrum and measures the depth of the feature to approximate
248 the amount of the mineral present (Swayze et. al., 2003). Benthic reflectance inversion
249 (Thompson *et al.*, 2017) and benthic cover classifier (Hochberg and Atkinson, 2003)
250 which we refer to together as 'benethic cover classifier' and least squares (Dozier and
251 Painter, 2004) approaches rely on *in situ* data to determine which benthic cover type or
252 snow grain size a particular reflectance represents. PLSR also uses *in situ* data to derive
253 coefficients that are then applied to the reflectance to retrieve a vegetation property (e.g.,
254 leaf nitrogen mass fraction).

255

| Resolution | Core science area (Scene) | Algorithm | L3 retrieval (units) |
|---|---|---|---|
| Spectral | Mineral (Cuprite, Nevada, USA; AVIRIS-C; Swayze *et al.*, 2014) | Absorption feature matching | Mineral mass fraction (unitless; i.e., spectral abundance) |
| | Aquatic (Arlington, Great Barrier Reef, Australia; DESIS; German Aerospace Center) | Benthic cover classifier | Benthic cover type (unitless) |
| | Vegetation (Western Ghants, South India; Zheng *et al.* In Review) | Partial least squares regression | Leaf nitrogen mass fraction (g/mg) |
| | Snow (Southern Rocky Mountains, USA; Skiles and Painter, 2017) | Least squares | Snow grain size (μm) |
| Spatial | Vegetation (Western Ghants, South India; | Partial least squares regression | Leaf nitrogen mass fraction (g/mg) |

| | | | |
|---|---|---|---|
| | Zheng *et al.* In Review) | | |
| | Vegetation (Crested Butte, Colorado, USA; Chadwick *et al.*, 2020) | Partial least squares regression | Leaf nitrogen mass fraction (g/mg) |
| Temporal | Event detection (Simulation) | NA | Event (no units) |

**Table 1**: *Experiment List*. Each row describes the components of an experiment in our study grouped by the trade study resolution of interest. If citations are applicable, they are found in parentheses.

### 2.3 Temporal revisit

Acquisitions with high temporal revisit for hyperspectral data are rare in airborne (i.e., AVIRIS-NG) and spaceborne archives, including PRISMA and DESIS. Lack of high revisit hyperspectral data is problematic for assessing algorithm performance and expected event detection efficiency (Schimel, Townsend and Pavlick, 2020). To overcome this obstacle here to provide quantitative information for mission architecture design in terms of revisit, we use an analytical approach where we calculate event detection probability by dividing event duration by the revisit interval. The analytical study quantifies the amount of information missed by decreasing temporal resolution for disturbance events such as fires, volcanic eruptions or landslides, which have been listed as SBG designated observables (National Academies of Sciences, Engineering, and Medicine, 2018).

Satellite constellations have been proposed to increase revisit time intervals by increasing the number of instruments. We provide a brief analysis of uncertainty in a vegetation retrieval caused by instrument calibration drift. Calibration drift is the time between instrument calibration at an invariate site where the longer the time the more uncertainty from drift can be expected. For this analysis, we use calibration drift uncertainty estiamtes derived from AVIRIS-NG where we took a random draw from a multivariate normal with mean zero and covariance from the AVIRIS-NG estimate. We applied this draw linearly to a single radiance vector to represent how drift may increase uncertainty over time. From this set of radiances with increasing drift, we estimated surface reflectance using an ISOFIT inversion. Finally, we calculated the canopy nitrogen

content in the set of estimated reflectances using PLSR and compared the nitrogen estimates over days since calibration by calculating the relative error percentage.

## 3 Results

### 3.1 Spectral resolution

High spectral resolution (< 20 nm) resulted in greater algorithm accuracy across all scientific areas in the direct algorithm application (Figure 3). The 10 nm standard proposed by NASA Earth Sciences Decadal Survey (2017) provided the algorithm accuracy across experiments (Figure 3 vertical dotted line). On average, vegetation PLSR was the most sensitive to spectral resolution degradation, with an average RMSE change of 1.7 between experiments followed by the least squares snow grain size retrieval and the aquatic benthic cover classifier with an average of -8.78 and -7.38 change in kappa score respectively. Least squares (i.e., snow) appears to be the least sensitive to spectral resolution degradation.

Accuracy was not degraded significantly with the inclusion of instrument noise for the mineral or aquatic spectral resolution experiments (Figure 4). Both Instrument-A and Instrument-B had increased retrieval accuracy between 5nm and 10nm because of the tradeoffs between SNR and spectral resolution (Figure 4a). The vegetation retrievals were similar across spectral resolutions for Instrument-A and Instrument-B. However, Hyperion performed poorly (i.e., RMSE = 23.54 mg/g; Figure 4b). The benthic cover classifier for the aquatic spectral resolution experiment incorrectly classified the majority of pixels at low spectral resolutions, classifying all pixels as algae (Figure 4c). This convergence to algae classification caused a dip in the 20 nm spectral resolution experiment). For the snow algorithm, SNR degraded algorithm accuracy across spectral resolution experiments for both Instrument-A, Instrument-B, and Hyperion (Figure 4d).

Approximately 20% of the snow spectra were categorized as having the highest snow grain size in each of the instrument application experiments.

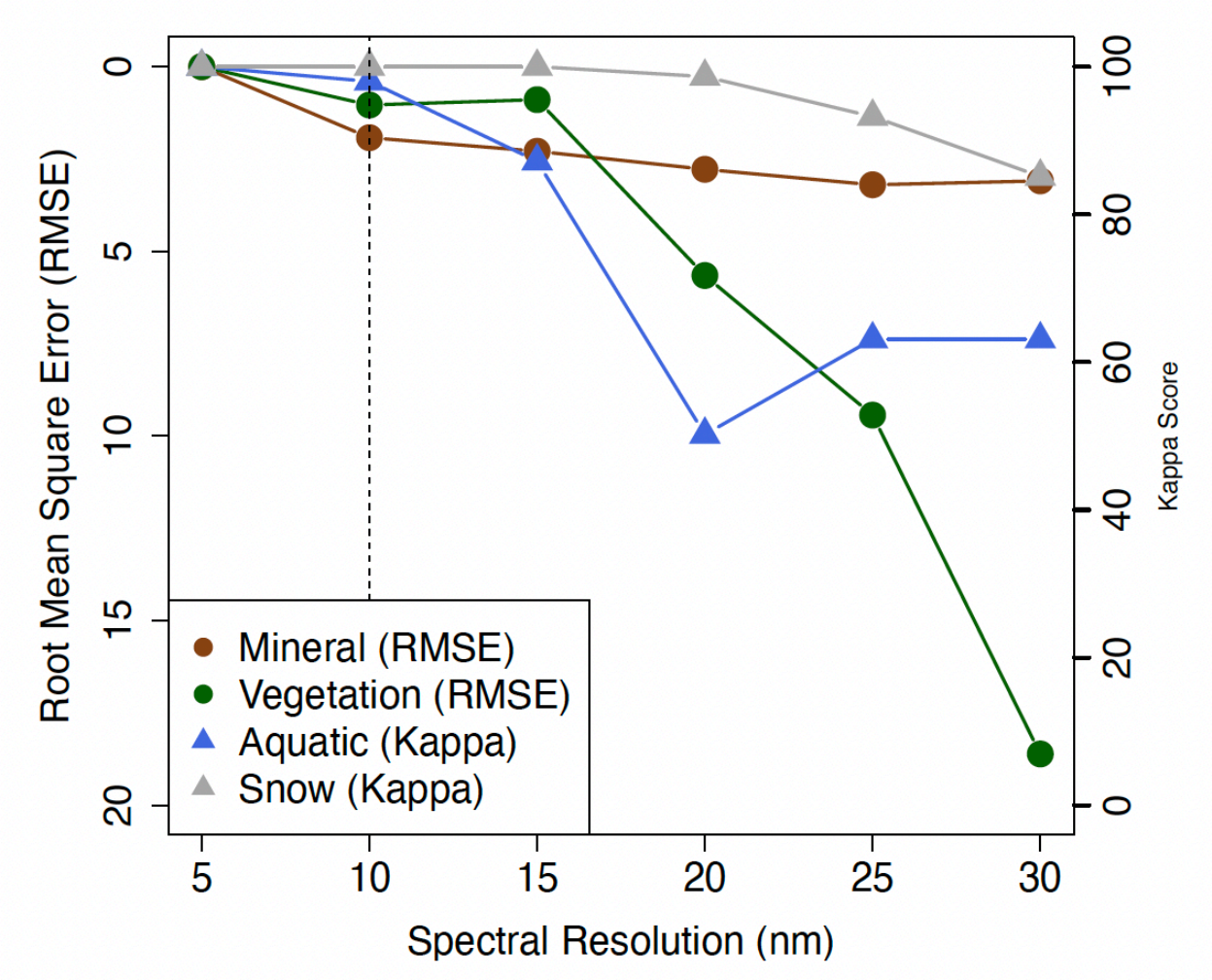


**Figure 3**: Direct application algorithm accuracy across spectral resolution colored by scientific area. These retrievals were calculated using true reflectance and each of the retrieval algorithms. Root mean square error (RMSE) was calculated for mineral and vegetation spectra while kappa score was calculated for aquatic and snow spectra. Vertical lines represent spectral resolution

312 targets defined by the National Academies' 2017 Decadal Survey on Earth Science and
313 Applications.

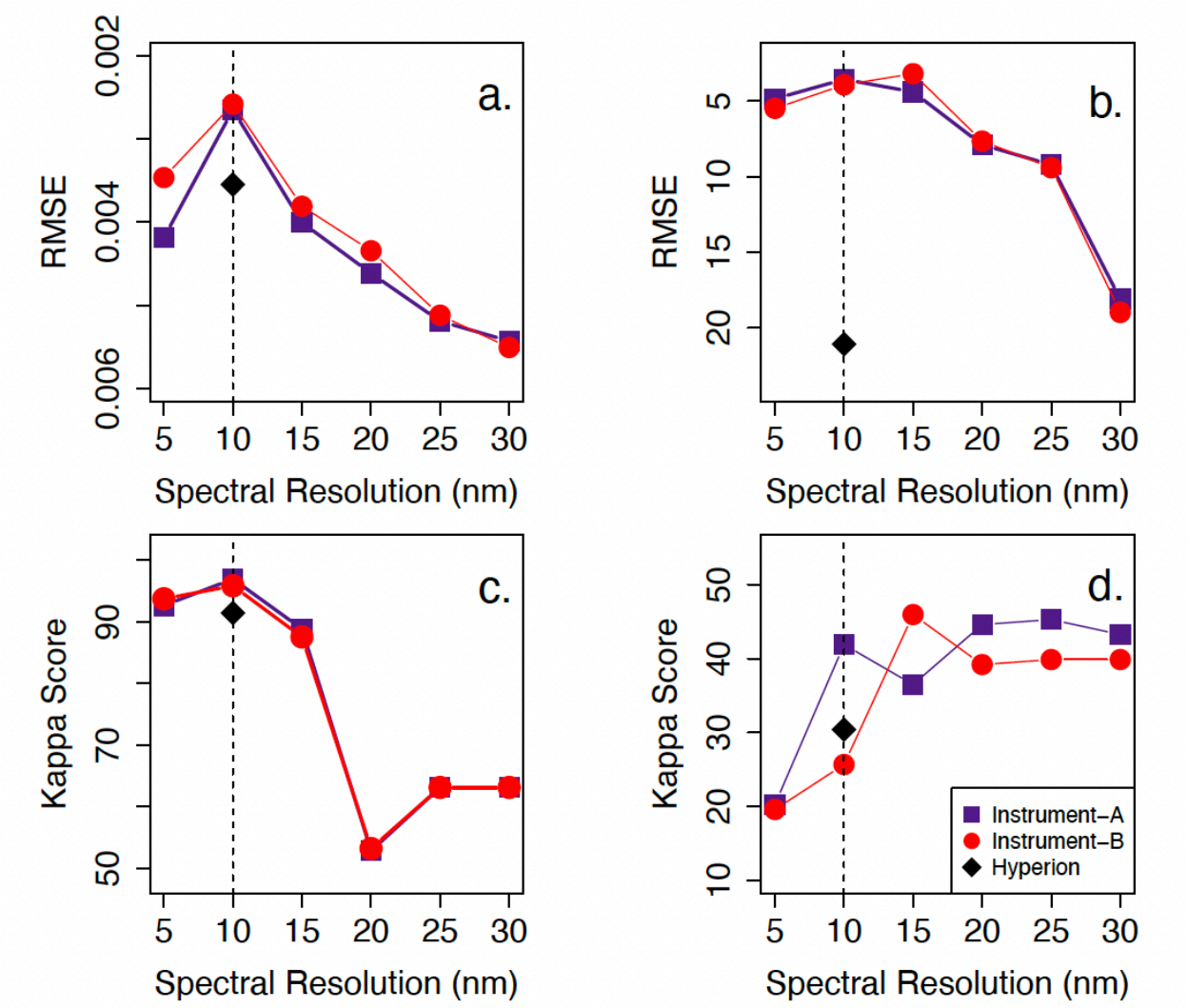


314

315 **Figure 4**: Instrument application algorithm accuracy across spectral resolution colored by
316 scientific area for Instrument-A (purple), Instrument-B (red), and Hyperion (black) for mineral
317 (a), vegetation (b), aquatic (c), and snow (d) retrivals. Root mean square error (RMSE) was
318 calculated for mineral and vegetation spectra while kappa score was calculated for aquatic and
319 snow spectra. Vertical lines represent spectral resolution targets defined by the National
320 Academies' 2017 Decadal Survey on Earth Science and Applications.

321 3.2 Spatial resolution

322 Retrieval accuracy decreased with coarsening spatial resolutions for both the Colorado
323 and the South India sites in the direct application of the vegetation algorithms. Retrieval
324 accuracy declined more quickly in the heterogeneous Colorado scene than the
325 homogeneous South India scene (black versus green Figure 5). The 30 m standard
326 proposed by NASA Earth Science Decadal Survey (2017) provided the most algorithm

accuracy across experiments (Figure 5 vertical dotted line). There was a slight increase in retrieval accuracy in the state of Colorado scene between the 50 m and 60 m spatial resolution experiments. We assumed this was caused by spectral mixing between vegetated and non-vegetated spectra within a heterogenous scene (Figure S3).

Instrument-A, Instrument-B, and Hyperion applications that included the affects of noise both greatly decreased retrieval accuracy compared to the direct applications (Figure 6). Increasing SNR over decreasing spatial resolution caused accuracy to increase somewhat for both Instrument-A and Instrument-B applications, especially between 20 m and 30 m spatial resolution experiments. Average SNR increased in the SWIR between instruments configured for 20 m to 30 m spatial resolution by 78% SNR for Instrument-A and 81% SNR for Instrument-B (Figure 1, dark purple). Hyperion was most sensitive to the PLSR algorithm (Figure 4b). In comparison to both Instrument-A and Instruement-B, Hyperion poorly estimated canopy nitrogen content.

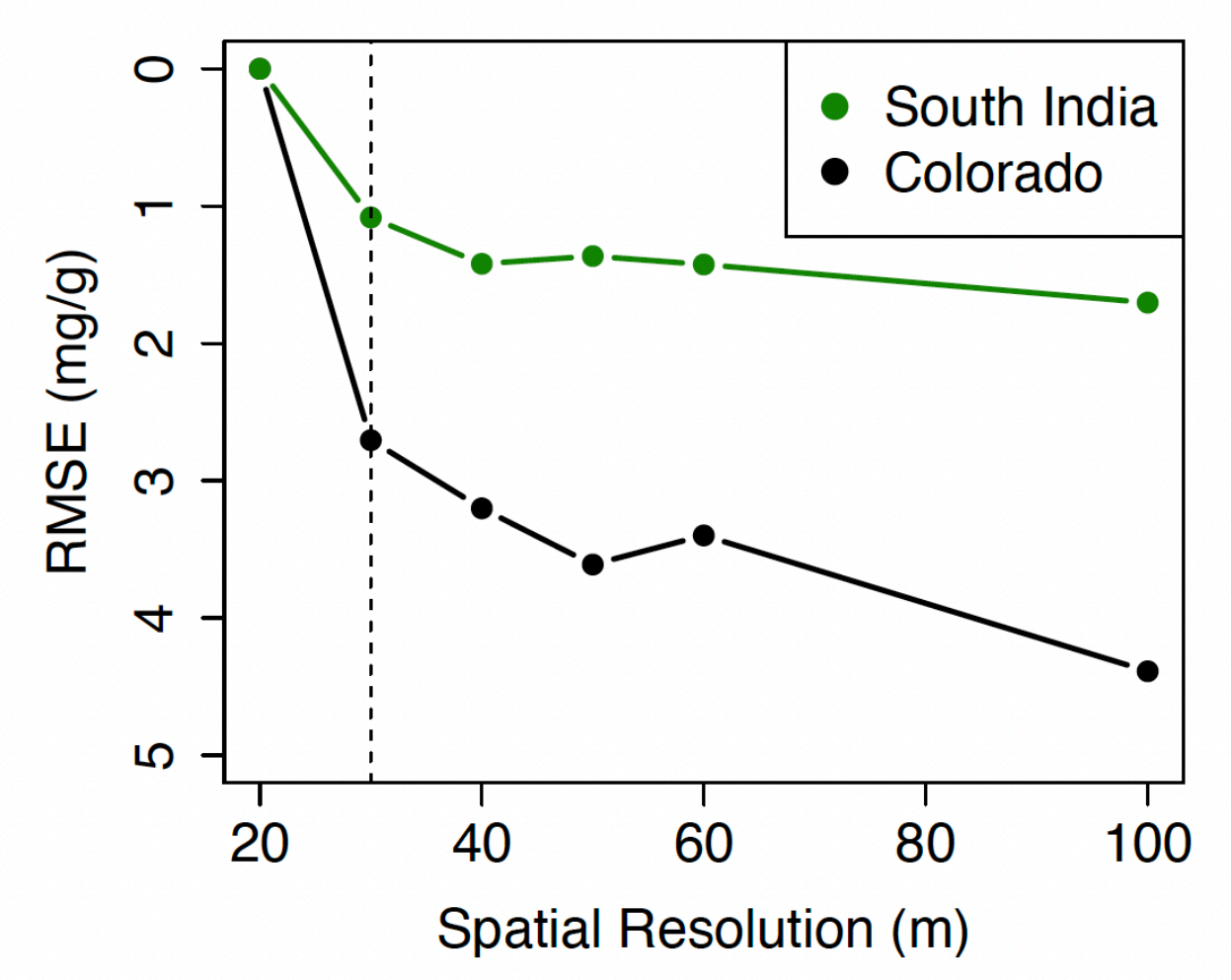


**Figure 5**: Direct application algorithm accuracy calculated by root mean square error (RMSE) between the degraded resolution and the native resolution across spatial resolution experiments

colored by scene. Vertical lines represent spectral resolution targets defined by the National Academies' 2017 Decadal Survey on Earth Science and Applications.

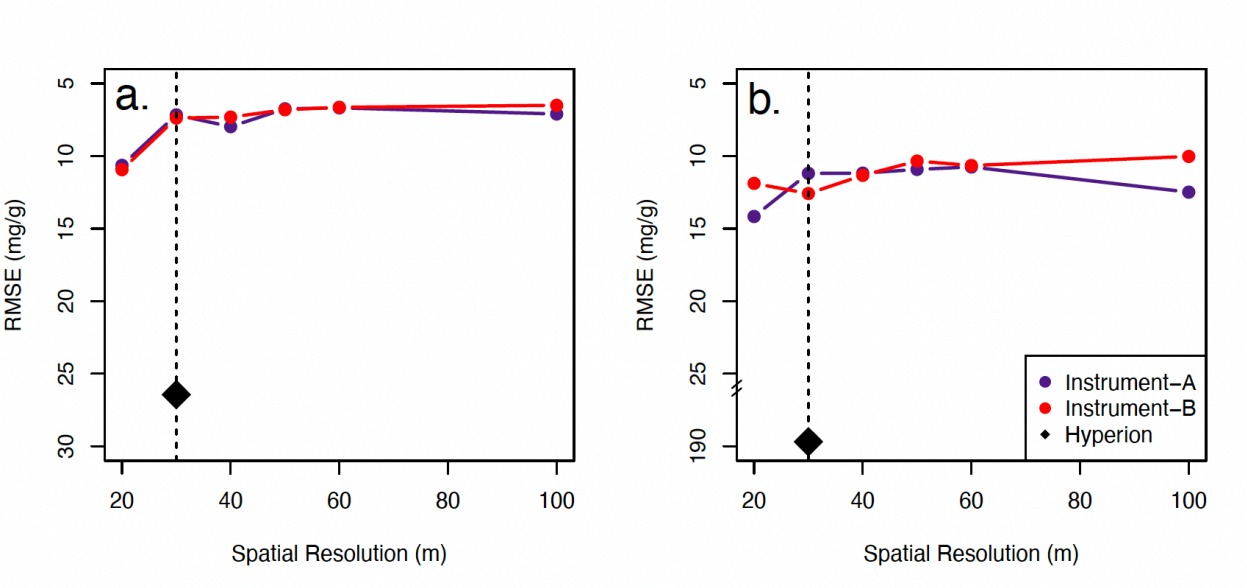


**Figure 6**: Instrument application algorithm accuracy for South India (a) and Colorado (b) scenes. The instrument application includes the effects of noise on retrieval accuracy while the direct application (Figure 5) does not. Hyperion noise (black diamond) caused large inaccuracy in both vegetation retrievals, but especially in the Colorado scene (b). We have broken the vertical axis to include this point. Vertical lines represent spectral resolution targets defined by the National Academies' 2017 Decadal Survey on Earth Science and Applications.

### 3.3 Temporal resolution (revisit)

Mission revisit cadence greatly affected the probability of detecting short term events (Figure 7). Revisiting more than 20 days for a short-term event (< 5 days in duration) resulted in a probability of detection of less than 20%. Long duration events (> 21 days in duration) had a higher probability of detection even for greater than 60 day revisits (probability > 40%). Lastly, calibration drift decayed retrival accuracy (Figure 8). Percent error reached 60% in 175 days since calibration and 100% in 300 days since calibration.

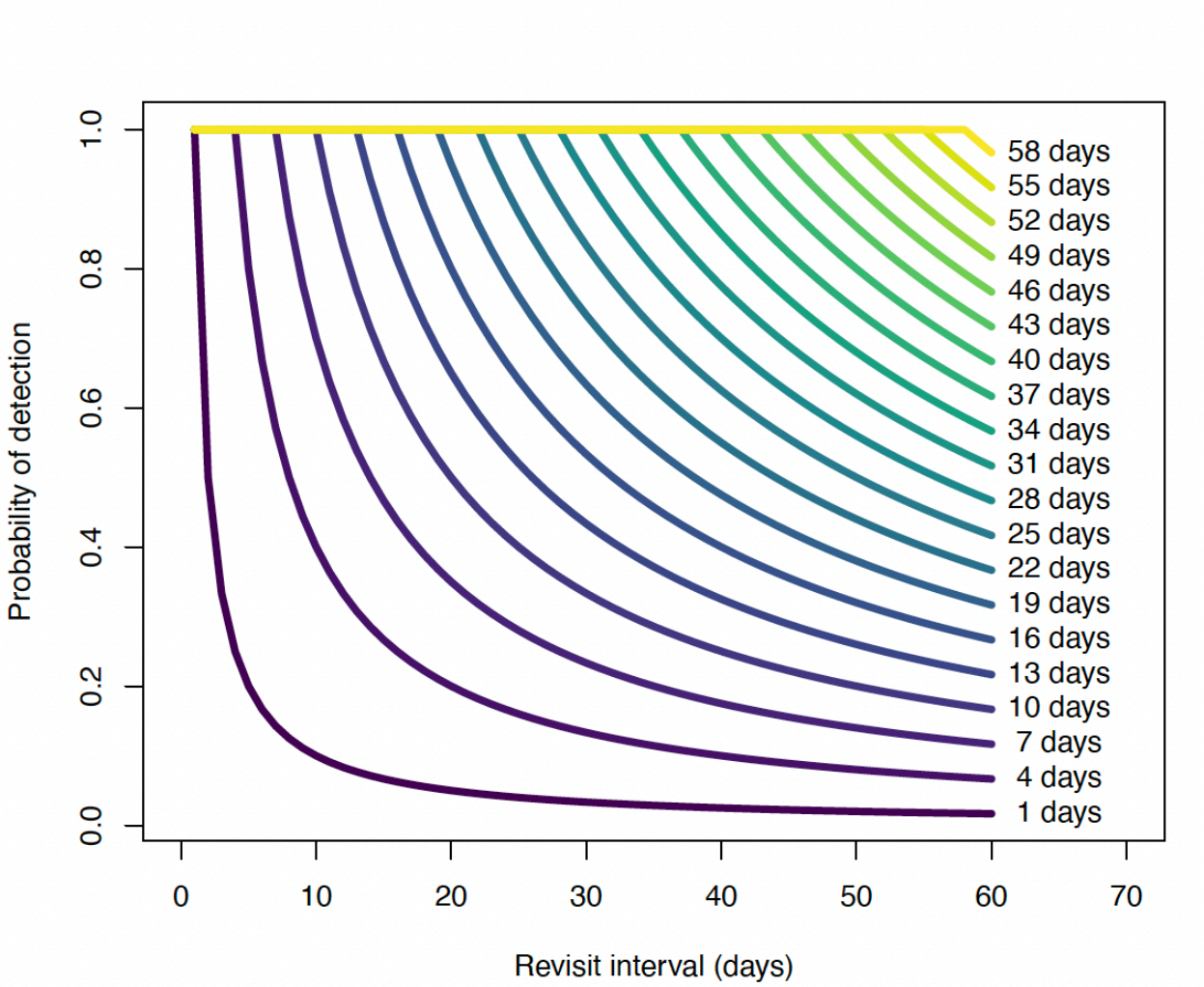


360

361 **Figure 7**: Detection probability as a function of increasing revisit interval colored by the
362 duration of the event where shorter events are more difficult to detect with higher revisit time
363 intervals.

364

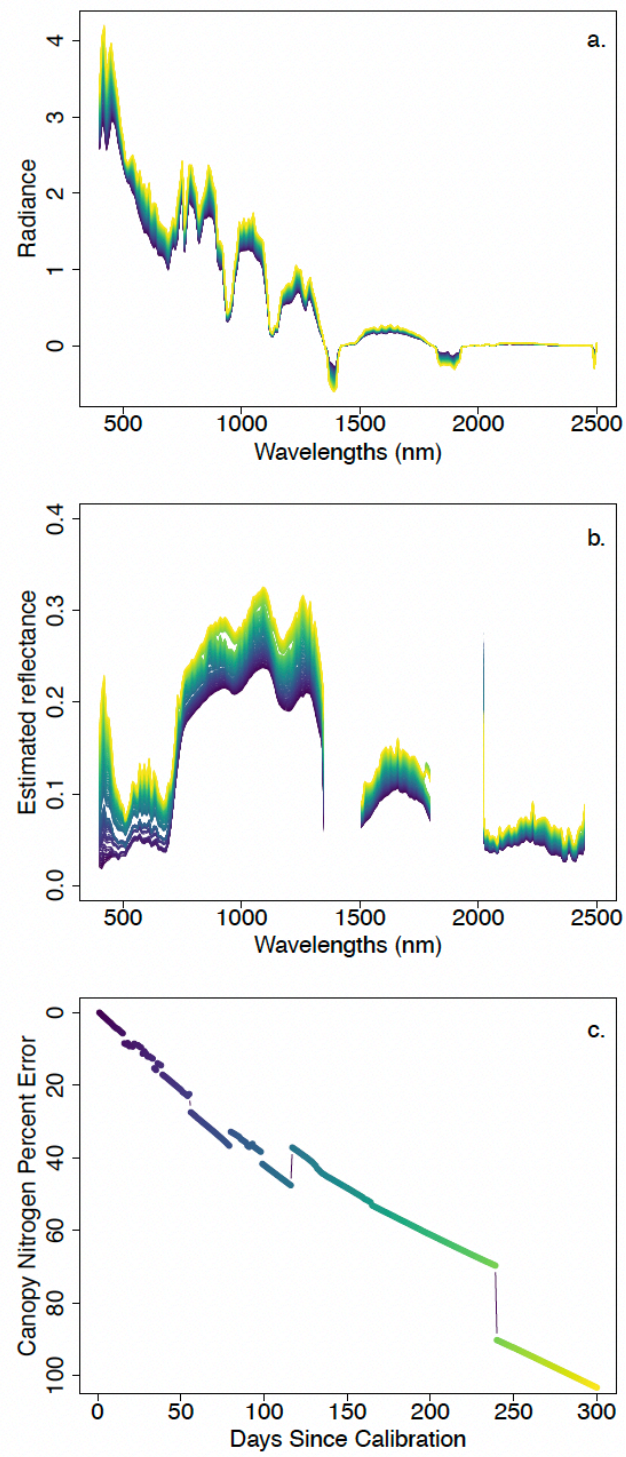


365

366 **Figure 8**: a. Example radiances with increasing error due to drift or days since calibration. b.
367 Estimated reflectances of the radiances in (a). c. canopy nitrogen percent error as a function of
368 days since calibration. Colors in a, b, and c correspond to days since calibration.

369 **4 Discussion**

This suite of driving cases covering three aspects (i.e., spectral, spatial, and revisit) of mission architecture interlinked with SNR and four of the five core science areas shows where high resolution requirements are necessary to preserve algorithm accuracy. Our analyses confirm that high spectral (~10nm), high spatial (~30m), and high revisit (less than 16 days) is needed to effectively quantitatively constrain Earth's geophysical property estimation with hyperspectral imagery and corresponding retrieval algorithms. We represent these targets with Figure 3 through 6 vertical dotted lines. Specifically, instruments with spatial resolution of 30 m and spectral resolution of 10 nm obtain the largest accuracies, across the five scientific foci explored here. This largely corroborates the performance proposed by the Decadal Survey in their original description of the SBG mission concept. We also highlight the difference between instrument choices Instrument-A and Instrument-B and past instrument Hyperion to showcase how the instrument selection process may be informed by simulation experiments using hypertrace or similar mission design workflows. Overall, the instruments performed similarly and outperformed Hyperion (See Figure 4 and Figure 6). In the following paragraphs, we elaborate on our findings for each type of resolution and finally describe our vision for the future of NASA mission architecture studies.

We build upon previous research of mineral and vegetation retrieval algorithms (Swayze et al, 2003; Kokaly et al 2009; Shiklomanov *et al.*, 2016) showing that high spectral resolution (~10nm) improved retrieval estimation across all scientific areas (Figure 3). In our mineral assessment, we used Kaolinite absorption feature matching. This retrieval algorithm depends on a narrow range of wavelengths (i.e., 2100nm - 2300nm). As the spectral resolution is coarsened, the number of data points within this range decreases rapidly and results in an exponential loss of information over spectral resolution. Similarly, least squares spectral matching uses a spectral library as a reference for determining the amount of snow in a pixel (Dozier and Painter, 2004). Aquatic benthic cover classification and vegetation PLSR algorithms use coefficients that are empirically estimated using *in situ* and concurrently measured hyperspectral data, and are then applied to remotely sensed imaging spectrometer data (Thompson, Hochberg, *et al.*, 2017; Serbin and Townsend, 2020; Cawse-Nicholson, et al 2019) The *in situ* data are collected at a particular spectral and spatial resolutions at particular locations usually during the summer months with both airborne and in site data, which may ultimately drive the sensitivity of these algorithms to degrading spectral resolution (e.g., Hochberg and Atkinson, 2003). More work is needed to understand what the optimal sampling scheme is for both *in situ* and remotely sensed hyperspectral data and how to use these data in tandem for improving aquatic classifications and vegetation trait estimation algorithm retrievals.

Increased spatial resolution is a particularly important component for vegetation research because plants operate on individual plant scales and aggregate and interact at ecosystem scale to drive Earth system level phenomena (e.g., individual spruce tree to the boreal forest). Earth system scientists are increasingly arguing for representing cohorts or individual level plant traits and processes at a large scale to inform Earth system models (Fisher *et al.*, 2018). SBG would greatly influence these models by providing a large-scale dataset at a relevant level of plant organization (i.e., ~30m; Malenovsky et al, 2019). We show (Figure 4) a quantitative threshold for spatial resolution from the vegetation algorithm perspective. However, both mission and instrument design must be carefully constructed to include high spatial resolution and accommodate physical barriers that may decrease the SNR. For the same instrument and global coverage, narrower swath/field-of-view means better spatial resolution and more consistent

angular sampling but worse temporal resolution. So, an advance in spatial resolution may mean compromising in temporal resolution. Coordinated international collaborations with other global imaging spectroscopy missions (e.g. Eurpean Space Agency's Copernicus Hyperspectral Imaging Mission) might provide a path forward for meeting high revisit science requirements while also improving spatial resolution. Future work may focus on understanding how high spatial resolution multispectral imagery informs lower spatial resolution hyperspectral trait estimation to ultimately improve global vegetation trait data.

Altering the orbiting altitude of an instrument with a particular spatial resolution configuration can increase SNR by allowing more photons to be received from a particular pixel. But, a particular orbiting altitude with longer revisit intervals may not be desirable for short duration event detection (Figure 6, dark purple). While our assessment relies on simulated data, it is clear that increased revisit will increase the probability that events such as volcanic eruptions or mudslides are detected by SBG. Extreme events are increasing with frequency as the climate changes (NASA ESAS, 2016) and the effects of these types of events may be some of the most important aspects of mission design to the public. Furthermore, our analysis is optimistic as it did not include a source of clouds where the presence of clouds will lead to missing data and in turn longer revisit. Higher revisit will enable a higher probability that any image is taken because it will be more likely that an overpass occurs on a clear or semi-clear day. While satellite constellations may help improve the revisit interval, the calibration drift greatly affects retrieval accuracy (Figure 8) and would need to be included in the uncertainty propagration of retrievals from satellite consteallations.

The SBG mission is driven by the ideals of the decadal survey, striving to better understand the changing geophysical properties across the Earth system (National Academies of Sciences, Engineering, and Medicine, 2019). We have shown the dominant components that drive retrieval uncertainty across four core scientific areas. Our approach utilizes a workflow for simulating the SNR effects of mission instruments and includes many aspects of data processing uncertainties. Future work may focus on using this type of setup for mission planning where simulations may be run to parse out different dominant contributors of uncertainty. For example, intrinsic dimensionality can provide an algorithm agnostic evaluation approach by focusing simply on information content (Cawse-Nicholson et. al, 2019). Once the mission design has been finalized our method can be used to inform the data pipeline from SBG or future hyperspectral missions by applying realistic uncertainties along the data processing steps.

## Acknowledgments

Some of the research described in this paper was carried out at the Jet Propulsion Laboratory, California Institute of Technology, under contract with the National Aeronautics and Space Administration. Government sponsorship acknowledged. We acknowledge funding from NASA's Surface Biology and Geology Designated Observable.

## Open Research Statement

The data used in this work are hyperspectral images collected from past published works (Listed in Table 1). The software used in this work is ISOFIT (https://doi.org/10.5281/ZENODO.4614338), HYPERTRACE

457 (https://github.com/isofit/isofit/tree/master/examples/py-hypertrace), and four types of
458 hyperspectral algorithms (See Table 1).

459 **References**

460 Bioucas-Dias, J. M., & Nascimento, J. M. P. (2005). Estimation of signal subspace on hyperspectral data.
461 In L. Bruzzone (Ed.) (p. 59820L). Presented at the Remote Sensing, Bruges, Belgium.
462 https://doi.org/10.1117/12.620061

463 Burnett, A. C., Anderson, J., Davidson, K. J., Ely, K. S., Lamour, J., Li, Q., et al. (2021). A best-practice
464 guide to predicting plant traits from leaf-level hyperspectral data using partial least squares
465 regression. Journal of Experimental Botany, 72(18), 6175–6189. https://doi.org/10.1093/jxb/erab295

466 Cavender-Bares, J., Gamon, J. A., & Townsend, P. A. (Eds.). (2020). Remote sensing of plant
467 biodiversity. Cham: Springer.

468 Cawse-Nicholson, K., Hook, S. J., Miller, C. E., & Thompson, D. R. (2019). Intrinsic Dimensionality in
469 Combined Visible to Thermal Infrared Imagery. IEEE Journal of Selected Topics in Applied Earth
470 Observations and Remote Sensing, 12(12), 4977–4984. https://doi.org/10.1109/JSTARS.2019.2938883

471 Cawse-Nicholson, K., Townsend, P. A., Schimel, D., Assiri, A. M., Blake, P. L., Buongiorno, M. F., et al.
472 (2021). NASA's surface biology and geology designated observable: A perspective on surface imaging
473 algorithms. Remote Sensing of Environment, 257, 112349. https://doi.org/10.1016/j.rse.2021.112349

474 Chadwick, K. D., Brodrick, P. G., Grant, K., Goulden, T., Henderson, A., Falco, N., et al. (2020).
475 Integrating airborne remote sensing and field campaigns for ecology and Earth system science. Methods
476 in Ecology and Evolution, 11(11), 1492–1508. https://doi.org/10.1111/2041-210X.13463

477 Committee on Extreme Weather Events and Climate Change Attribution, Board on Atmospheric Sciences
478 and Climate, Division on Earth and Life Studies, & National Academies of Sciences, Engineering, and
479 Medicine. (2016). Attribution of Extreme Weather Events in the Context of Climate Change. Washington,
480 D.C.: National Academies Press. https://doi.org/10.17226/21852

481 Connelly, D. S., Thompson, D. R., Mahowald, N. M., Li, L., Carmon, N., Okin, G. S., & Green, R. O.
482 (2021). The EMIT mission information yield for mineral dust radiative forcing. Remote Sensing of
483 Environment, 258, 112380. https://doi.org/10.1016/j.rse.2021.112380

484 Curran, P. J. (1989). Remote sensing of foliar chemistry. Remote Sensing of Environment, 30(3), 271–
485 278. https://doi.org/10.1016/0034-4257(89)90069-2

486 Dierssen, H. M. (2021). Corrigendum: Hyperspectral Measurements, Parameterizations, and Atmospheric
487 Correction of Whitecaps and Foam From Visible to Shortwave Infrared for Ocean Color Remote
488 Sensing. Frontiers in Earth Science, 9, 683136. https://doi.org/10.3389/feart.2021.683136

489 Dozier, J., & Painter, T. H. (2004). Multispectral and hyperspectral remote sensing of alpine snow
490 properties. Annual Review of Earth and Planetary Sciences, 32(1), 465–494.
491 https://doi.org/10.1146/annurev.earth.32.101802.120404

492 Garcia, R. A., Lee, Z., Barnes, B. B., Hu, C., Dierssen, H. M., & Hochberg, E. J. (2020). Benthic
493 classification and IOP retrievals in shallow water environments using MERIS imagery. Remote Sensing
494 of Environment, 249, 112015. https://doi.org/10.1016/j.rse.2020.112015

German Aerospace Center (DLR). Available at: https://geoservice.dlr.de/data-assets/hxom21uqeo90.html (Accessed: 8 December 2021).

Hu, C. (2011). An empirical approach to derive MODIS ocean color patterns under severe sun glint. Geophysical Research Letters, 38(1), n/a-n/a. https://doi.org/10.1029/2010GL045422

Isofit, Brodrick, P., Erickson, A., Jfahlen, Winstonolson, Thompson, D. R., et al. (2021). isofit/isofit: 2.8.0 (Version v2.8.0). Zenodo. https://doi.org/10.5281/ZENODO.4614338

Kokaly, R. F., Asner, G. P., Ollinger, S. V., Martin, M. E., & Wessman, C. A. (2009). Characterizing canopy biochemistry from imaging spectroscopy and its application to ecosystem studies. Remote Sensing of Environment, 113, S78–S91. https://doi.org/10.1016/j.rse.2008.10.018

National Academies of Sciences, Engineering, and Medicine (U.S.), National Academies of Sciences, Engineering, and Medicine (U.S.), & National Academies of Sciences, Engineering, and Medicine (U.S.) (Eds.). (2018). Thriving on our changing planet: a decadal strategy for Earth observation from space. Washington, DC: The National Academies Press.

Nolin, A. W., & Dozier, J. (1993). Estimating snow grain size using AVIRIS data. Remote Sensing of Environment, 44(2–3), 231–238. https://doi.org/10.1016/0034-4257(93)90018-S

Schaepman-Strub, G., Schaepman, M. E., Painter, T. H., Dangel, S., & Martonchik, J. V. (2006). Reflectance quantities in optical remote sensing—definitions and case studies. Remote Sensing of Environment, 103(1), 27–42. https://doi.org/10.1016/j.rse.2006.03.002

Schimel, D., Townsend, P. A. and Pavlick, R. (2020) 'Prospects and Pitfalls for Spectroscopic Remote Sensing of Biodiversity at the Global Scale', in Cavender-Bares, J., Gamon, J. A., and Townsend, P. A. (eds) *Remote Sensing of Plant Biodiversity*. Cham: Springer International Publishing, pp. 503–518.

Serbin, Shawn P., and Philip A. Townsend. "Scaling functional traits from leaves to canopies." *Remote Sensing of Plant Biodiversity*. Springer, Cham, 2020. 43-82.

Stavaros et al. (In Review) 'Designing an Observing System to Study the Surface Biology and Geology of the Earth in the 2020s', *Journal of Geophysical Research: Biogeosciences*

Shiklomanov, A. N., Dietze, M. C., Viskari, T., Townsend, P. A., & Serbin, S. P. (2016). Quantifying the influences of spectral resolution on uncertainty in leaf trait estimates through a Bayesian approach to RTM inversion. Remote Sensing of Environment, 183, 226–238. https://doi.org/10.1016/j.rse.2016.05.023

Skiles, S. M., & Painter, T. (2017). Daily evolution in dust and black carbon content, snow grain size, and snow albedo during snowmelt, Rocky Mountains, Colorado. Journal of Glaciology, 63(237), 118–132. https://doi.org/10.1017/jog.2016.125

Song, C., Woodcock, C. E., Seto, K. C., Lenney, M. P., & Macomber, S. A. (2001). Classification and Change Detection Using Landsat TM Data. Remote Sensing of Environment, 75(2), 230–244. https://doi.org/10.1016/S0034-4257(00)00169-3

Swayze, G. A., Clark, R. N., Goetz, A. F. H., Livo, K. E., Breit, G. N., Kruse, F. A., et al. (2014). Mapping Advanced Argillic Alteration at Cuprite, Nevada, Using Imaging Spectroscopy. Economic Geology, 109(5), 1179–1221. https://doi.org/10.2113/econgeo.109.5.1179

Swayze, Gregg A. (2003). Effects of spectrometer band pass, sampling, and signal-to-noise ratio on

spectral identification using the Tetracorder algorithm. Journal of Geophysical Research, 108(E9), 5105. https://doi.org/10.1029/2002JE001975

Thompson, D. R., Boardman, J. W., Eastwood, M. L., & Green, R. O. (2017). A large airborne survey of Earth's visible-infrared spectral dimensionality. Optics Express, 25(8), 9186. https://doi.org/10.1364/OE.25.009186

Thompson, D. R., Hochberg, E. J., Asner, G. P., Green, R. O., Knapp, D. E., Gao, B.-C., et al. (2017). Airborne mapping of benthic reflectance spectra with Bayesian linear mixtures. Remote Sensing of Environment, 200, 18–30. https://doi.org/10.1016/j.rse.2017.07.030

Thompson, D. R., Natraj, V., Green, R. O., Helmlinger, M. C., Gao, B.-C., & Eastwood, M. L. (2018). Optimal estimation for imaging spectrometer atmospheric correction. Remote Sensing of Environment, 216, 355–373. https://doi.org/10.1016/j.rse.2018.07.003

Thompson, D. R., Bearden, D., Brosnan, I., Cawse-Nicholson, K., Chrone, J., Green, R. O., et al. (2021). NASA's Surface Biology and Geology Concept Study: Status and Next Steps. In 2021 IEEE International Geoscience and Remote Sensing Symposium IGARSS (pp. 112–114). Brussels, Belgium: IEEE. https://doi.org/10.1109/IGARSS47720.2021.9554480

Turner, M. G., Dale, V. H., & Gardner, R. H. (1989). Predicting across scales: Theory development and testing. Landscape Ecology, 3(3–4), 245–252. https://doi.org/10.1007/BF00131542

Vermote, E. F., & Kotchenova, S. (2008). Atmospheric correction for the monitoring of land surfaces. Journal of Geophysical Research, 113(D23), D23S90. https://doi.org/10.1029/2007JD009662

Verrelst, J., Malenovský, Z., Van der Tol, C., Camps-Valls, G., Gastellu-Etchegorry, J.-P., Lewis, P., et al. (2019). Quantifying Vegetation Biophysical Variables from Imaging Spectroscopy Data: A Review on Retrieval Methods. Surveys in Geophysics, 40(3), 589–629. https://doi.org/10.1007/s10712-018-9478-y

Wang, R., Gamon, J. A., Cavender-Bares, J., Townsend, P. A., & Zygielbaum, A. I. (2018). The spatial sensitivity of the spectral diversity–biodiversity relationship: an experimental test in a prairie grassland. Ecological Applications, 28(2), 541–556. https://doi.org/10.1002/eap.1669

Wang, Z., Chlus, A., Geygan, R., Ye, Z., Zheng, T., Singh, A., et al. (2020). Foliar functional traits from imaging spectroscopy across biomes in eastern North America. New Phytologist, 228(2), 494–511. https://doi.org/10.1111/nph.16711

Zheng, T. *et al.* (in prep) 'Variability in forest plant traits along the Western Ghats of India and their environmental drivers at different resolutions', *The New Phytologist*.